Microscopic and semimicroscopic analysis of the reaction ^{27}Al(p,α)^{24}Mg in the energy range between 20 and 45 MeV

F. Hoyler, H. Oberhummer,* T. Rohwer, and G. Staudt
Physikalisches Institut der Universität Tübingen, D-7400 Tübingen, Federal Republic of Germany

H. V. Klapdor
Max-Planck-Institut für Kernphysik, D-6900 Heidelberg, Federal Republic of Germany
(Received 10 January 1984; revised manuscript received 6 August 1984)

The microscopic model of the distorted-wave Born approximation theory for (p,α) reactions formulated in the isospin representation is compared with a semimicroscopic analysis using cluster form factors and SU(3) spectroscopic amplitudes. The differential cross sections of α particles emitted in the reaction ^{27}Al(p,α)^{24}Mg have been measured at the bombarding energies 20, 24, 30.5, and 45 MeV. The microscopic as well as the semimicroscopic distorted-wave Born approximation analysis reproduces the angular distributions in a large range of incident energies when using energy-dependent optical potentials. The relative intensities of the transitions to the ground state and excited states up to $E_x = 6$ MeV are described quite well in the semimicroscopic analysis.

I. INTRODUCTION

The application of the (p,α) and (α,p) reactions as a spectroscopic tool requires a semimicroscopic or microscopic description for this type of nuclear reaction. In the first microscopic analyses, harmonic oscillator single-particle wave functions were used.[1-3] Falk[4] has developed a microscopic model which uses the principle of expanding single-particle wave functions that are generated in a Woods-Saxon potential in terms of harmonic oscillator wave functions. Furthermore, a theory of three-particle transfer reactions which is derived from a generalization of the Bayman-Kallio method[5] of calculating the two-nucleon form factor has been presented by Smith[6] and Bayman *et al.*[7] The inclusion of finite-range effects to the microscopic theory has been performed by Falk *et al.*[8] and Oberhummer.[9] Furthermore, the microscopic model has been formulated in the isospin representation by Kunz *et al.*[10] and by Oberhummer *et al.*[11]

In the semimicroscopic formulation of three-nucleon transfer reactions the spectroscopic amplitude is calculated using the microscopic model, whereas for the form factor a cluster approximation is used. In this formalism the form factors are easy to calculate and result generally in better fits for the angular distributions.[6,12] A semimicroscopic model which includes coherence over configurations and intermediate couplings has been devised by Smits and Siemssen.[13] For nuclei in the 0*p* and 1*s* 0*d* shell another semimicroscopic model using the SU(3) scheme has been developed.[14-17] In this method the cluster spectroscopic factor is calculated in a simple manner. A number of (p,α) and (α,p) reactions has been analyzed in this way.[13,15,18,19]

The application of a cluster form factor in the semimicroscopic model results in angular distributions independent of the specific microscopic configurations. The shape of the angular distribution is only determined by the transferred total angular momentum J. This has been confirmed experimentally in the 0p shell.[20,21] On the other hand, in the *sd* shell some hints of shape differences in the angular distributions with the same J transfer are found,[22,23] suggesting an analysis using a microscopic form factor. Therefore, we have undertaken a series of (p,α) experiments in the *sd*-shell mass region.[19,23,24] The experimental data are compared with results of DWBA calculations in the microscopic description as well as in the semimicroscopic model using the SU(3) scheme. In order to make a comparison between these two methods feasible, the same set of shell-model wave functions has been used.

In this paper we present as a first result an analysis of the ^{27}Al(p,α)^{24}Mg reaction. Former work on this nucleus includes investigations of Kost and Hird[25] who have studied this reaction at 41 MeV with a simple cluster pickup model. In the work of Oberhummer *et al.*[11] this reaction has been investigated with polarized protons at $E_p = 34.73$ MeV.

In Secs. II A and II B we introduce a microscopic formulation of the DWBA theory for (p,α) reactions using the isospin formalism. We thereby use the method of performing a Talmi-Moshinsky transformation of the three-nucleon wave function in terms of harmonic-oscillator wave functions. Further details of the derivation of the expressions given below can be found in Ref. 11. In Sec. II C we calculate the transition amplitude using a cluster form factor and give the assumptions leading to the cluster approximation. In Sec. II D we discuss the calculation of spectroscopic amplitudes in the shell model and the SU(3) method of calculating cluster spectroscopic factors.

In Sec. III the experimental results are presented for the ^{27}Al(p,α)^{24}Mg reaction measured at four energies between 20 and 45 MeV. In Sec. IV the input data required for the DWBA calculations are summarized: in Sec. IV A the optical potential parameters are deduced from elastic scattering data, and in Secs. IV B and IV C the calculation of the form factors and the spectroscopic amplitudes are

described. In Sec. V the developed formalism is applied to the reaction ^{27}Al(p,α)^{24}Mg, and finally, the results are discussed.

II. FORMULATION OF THE DWBA THEORY

A. Transition amplitude with a microscopic form factor

The differential cross section for the reaction A(p,α)B can be written as

$$\frac{d\sigma}{d\Omega}=\frac{\mu_{pA}\mu_{\alpha B}}{(2\pi\hbar)^2}\frac{k_\alpha}{k_p}\frac{1}{(2s_p+1)(2J_A+1)}$$

$$\times\sum_{M_p M_A M_B}|T_{(p,\alpha)}(A,B)|^2 . \quad (1)$$

The quantities μ_{pA} and $\mu_{\alpha B}$ are the reduced masses in the entrance and exit channel, and $\vec{k}_p$ and $\vec{k}_\alpha$ are the relative momenta in these channels. The spin and magnetic quantum numbers of the projectile nucleon are s_p and M_p, respectively, whereas M_A and M_B are the magnetic quantum numbers of the target and residual nucleus.

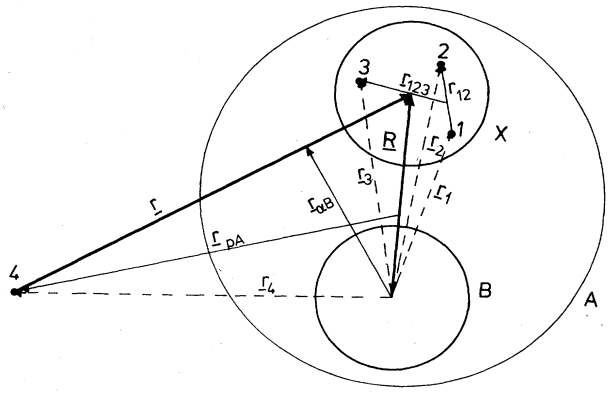

FIG. 1. Coordinates used in the three-nucleon transfer reaction.

The transition matrix is given in the DWBA by

$$T^{DWBA}_{(p,\alpha)}(A,B)=\int\int d\vec{R}\,d\vec{r}\,\chi^{(-)*}(\vec{k}_\alpha,\vec{r}_{\alpha B})\langle\psi_\alpha\psi_B\,|\,V\,|\,\psi_p\psi_A\rangle^a\chi^{(+)}(\vec{k}_p,\vec{r}_{pA}) . \quad (2)$$

In the expression for the transition amplitude the integration is carried out over the center-of-mass coordinate $\vec{R}=\frac{1}{3}(\vec{r}_1+\vec{r}_2+\vec{r}_3)$ and the relative coordinate $\vec{r}=\frac{1}{3}(\vec{r}_1+\vec{r}_2+\vec{r}_3)-\vec{r}_4$ between the projectile nucleon labeled 4 and the center of mass of the three transferred nucleons labeled 1, 2, and 3. The optical wave functions $\chi^{(+)}(\vec{k}_p,\vec{r}_{pA})$ and $\chi^{(-)}(\vec{k}_\alpha,\vec{r}_{\alpha B})$ in the entrance and exit channels are functions of the relative coordinates $\vec{r}_{pA}=(m_B/m_A)\vec{R}-\vec{r}$ and $\vec{r}_{\alpha B}=\vec{R}-(m_p/m_\alpha)\vec{r}$ in these channels (see Fig. 1).

The antisymmetrized nuclear matrix element with the superscript a

$$\langle\psi_\alpha\psi_B\,|\,V\,|\,\psi_p\psi_a\rangle^a=\binom{4}{3}^{1/2}\binom{A}{3}^{1/2}\langle\psi^a_\alpha\psi^a_B\,|\,V\,|\,\psi_p\psi^a_A\rangle \quad (3)$$

depends on the internal wave function of the projectile ψ_p, the ejectile ψ^a_α, the target nucleus ψ^a_A, and the residual nucleus ψ^a_B. The binominal coefficients

$$\binom{4}{3}^{1/2}$$

and

$$\binom{A}{3}^{1/2}$$

stem from the antisymmetrization procedure.[26]

In order to calculate the nuclear matrix element (3) we need the interaction potential responsible for the three-nucleon transfer

$$V=\sum_{i=1}^{3}V_{i4}(\vec{r}_{i4}) , \quad (4)$$

which is a sum over the effective nucleon-nucleon potentials $V_{i4}(\vec{r}_{i4})$ between the projectile nucleon 4 and the three transferred nucleons 1, 2, and 3. Also we need the antisymmetrized wave functions for the α particle, which can be split up into a space and spin isospin part

$$\psi^a_\alpha(\xi_1,\xi_2,\xi_3,\xi_4)=\varphi_\alpha(\vec{r}_1,\vec{r}_2,\vec{r}_3,\vec{r}_4)^{L_\alpha=0}_{M_{L_\alpha}=0}$$

$$\times\chi^a_\alpha(1,2,3,4)^{S_\alpha=T_\alpha=0}_{M_{s_\alpha}=N_\alpha=0} . \quad (5)$$

The wave function of the target nucleus ψ^a_A can be expanded in the JT representation with the wave functions of the residual nucleus and the three transferred nucleons

$$\psi^a_A(\xi_A)^{J_A T_A}_{M_A N_A}=\binom{A}{3}^{-1/2}\sum_{\substack{JJ_B\\TT_B}}\sum_{\rho}S^{1/2}_{AB}(\rho JT)[\psi^a_B(\xi_B)^{J_B T_B}\times\psi^a_x(\xi_1,\xi_2,\xi_3)^{\rho JT}]^{J_A T_A}_{M_A N_A} , \quad (6)$$

where the cross product is defined as

$$[\psi^a_B(\xi_B)^{J_B T_B}\times\psi^a_x(\xi_1,\xi_2,\xi_3)^{\rho JT}]^{J_A T_A}_{M_A N_A}\equiv\sum_{M_B M}\sum_{N_B N}\langle J_B M_B JM\,|\,J_A M_A\rangle\langle T_B N_B TN\,|\,T_A N_A\rangle$$

$$\times\psi^a_B(\xi_B)^{J_B T_B}_{M_B N_B}\psi^a_x(\xi_1,\xi_2,\xi_3)^{\rho JT}_{MN} \quad (7)$$

and ρ represents all internal quantum numbers necessary to characterize the three transferred nucleons. The ξ_A and ξ_B are the internal coordinates of the target nucleus A and the residual nucleus B. The $\xi_i \equiv (\vec{r}_i, \sigma_i, \tau_i)$ with $i=1$, 2, and 3 are the space, spin, and isospin single-particle coordinates of the three nucleons with $\vec{r}_i$ having their origins in the center of mass of the core B. The expansion coefficients $S_{AB}^{1/2}(\rho JT)$ are the spectroscopic amplitudes as discussed in Sec. II D.

The antisymmetrized three-particle wave function can be written as

$$\psi_x^a(\xi_1,\xi_2,\xi_3)_{MN}^{\rho JT} = N(\rho) Z(\rho) \psi_x(\xi_1,\xi_2,\xi_3)_{MN}^{\rho JT} , \tag{8}$$

where $N(\rho)$ and $Z(\rho)$ are the normalization and antisymmetrization factors given in Ref. 11. The three-particle wave function can be split up into a space and spin-isospin dependent part by transforming from the jj to the LS representation using two $9j$ symbols

$$\psi_x(\xi_1,\xi_2,\xi_3)_{MN}^{\rho JT} = \sum_{LS} \sum_{L_{12}S_{12}} \begin{bmatrix} l_1 & \frac{1}{2} & j_1 \\ l_2 & \frac{1}{2} & j_2 \\ L_{12} & S_{12} & J_{12} \end{bmatrix} \begin{bmatrix} L_{12} & S_{12} & J_{12} \\ l_3 & \frac{1}{2} & j_3 \\ L & \frac{1}{2} & J \end{bmatrix} [\varphi_x(\vec{r}_1,\vec{r}_2,\vec{r}_3)^{\rho L} \times \chi_x(1,2,3)^{\rho ST}]_{MN}^{JT} . \tag{9}$$

By inserting (5)—(9) into the expression for the nuclear matrix element (3), we can split up this matrix element into a space part and a spin-isospin part. The spin-isospin part can be calculated using spin algebra. In this way we obtain for the transition amplitude

$$\begin{aligned} T_{(p,\alpha)}^{DWBA}(A,B) = (\tfrac{4}{3})^{1/2} \sum_{JM} & \langle J_B M_B JM \mid J_A M_A \rangle \langle T_B N_B \tfrac{1}{2}(-\tfrac{1}{2}) \mid T_A N_A \rangle \\ & \times \sum_L \langle L(M+M_p)\tfrac{1}{2}(-M_p) \mid JM \rangle \langle \tfrac{1}{2} M_p \tfrac{1}{2}(-M_p) \mid 00 \rangle \langle \tfrac{1}{2}\tfrac{1}{2}\tfrac{1}{2}(-\tfrac{1}{2}) \mid 00 \rangle \\ & \times \sum_{\rho} \sum_{L_{12}S_{12}} (-1)^{T_{12}} \frac{1}{\sqrt{2}} \delta_{S_{12}+T_{12},1} g(\rho) \begin{bmatrix} l_1 & \frac{1}{2} & j_1 \\ l_2 & \frac{1}{2} & j_2 \\ L_{12} & S_{12} & J_{12} \end{bmatrix} \begin{bmatrix} L_{12} & S_{12} & J_{12} \\ l_3 & \frac{1}{2} & j_3 \\ L & \frac{1}{2} & J \end{bmatrix} S_{AB}^{1/2}(\rho JT) \\ & \times \int\int d\vec{R}\, d\vec{r}\, \chi^{(-)*}(\vec{k}_\alpha, \vec{r}_{\alpha B}) F_{M_L}^{\rho L}(\vec{R},\vec{r}) \chi^{(+)}(\vec{k}_p, \vec{r}_{pA}) , \end{aligned} \tag{10}$$

where the configuration factor $g(\rho)$ comes from the antisymmetrization and normalization procedure.[11]

B. Microscopic form factor

The form factor $F_{M_L}^{\rho L}(\vec{R},\vec{r})$ is defined as the space part of the nuclear matrix element

$$F_{M_L}^{\rho L}(\vec{R},\vec{r}) = \left\langle \varphi_\alpha(\vec{r}_1,\vec{r}_2,\vec{r}_3,\vec{r}_4)_0^0 \left| \sum_{i=1}^{3} V_{i4}(\vec{r}_{i4}) \right| \varphi_x(\vec{r}_1,\vec{r}_2,\vec{r}_3)_{M_L}^{\rho L} \right\rangle . \tag{11}$$

In order to calculate this form factor we have to transform from the coordinates $(\vec{r}_1,\vec{r}_2,\vec{r}_3,\vec{r}_4)$ to the new coordinates $\vec{R},\vec{r},\vec{r}_{12}=\vec{r}_2-\vec{r}_1$ and $\vec{r}_{123}=\vec{r}_3-\frac{1}{2}(\vec{r}_1+\vec{r}_2)$ shown in Fig. 1.

The α-particle wave function is assumed to have a Gaussian form[27]

$$\varphi_\alpha(\vec{r}_1,\vec{r}_2,\vec{r}_3,\vec{r}_4)_0^0 = \left[\frac{128\eta^6}{\pi^3} \right] \exp\left[-\eta^2 \sum_{i<j} (r_i - r_j)^2 \right] \tag{12}$$

with a size parameter $\eta = 0.233$ fm^{-1}, which is correlated to the equivalent harmonic oscillator constant $\nu_\alpha = 0.434$ fm^{-2} by $\eta^2 = \frac{1}{8}\nu_\alpha$ and to the rms radius of the α particle by $\langle r^2 \rangle^{1/2} = 3/8\eta = 1.61$ fm. Performing the coordinate transformation we obtain[28]

$$\begin{aligned} \varphi_\alpha(\vec{r}_1,\vec{r}_2,\vec{r}_3,\vec{r}_4)_0^0 &= \varphi_\alpha^{(1)}(\vec{r}) \varphi_\alpha^{(2)}(\vec{r}_{12},\vec{r}_{123}) \\ &= \left[\frac{3\nu_\alpha}{4\pi} \right]^{3/4} \exp[-\nu_\alpha(\tfrac{3}{8} r^2)] \left[\frac{\nu_\alpha^2}{3\pi^2} \right]^{3/4} \exp[-\nu_\alpha(\tfrac{1}{4} r_{12}^2 + \tfrac{1}{3} r_{123}^2)] . \end{aligned} \tag{13}$$

The interacting potential is also assumed to have a Gaussian form

$$\sum_{i=1}^{3} V_{i4}(\vec{r}_{i4}) = U_0 \sum_{i=1}^{3} \exp[-\beta^2(\vec{r}_4 - \vec{r}_i)^2] \,, \tag{14}$$

with $U_0 = 70$ MeV and $\beta = 0.632$ fm^{-1}.[29] For this potential we transform to the new coordinates by performing the Chant-Mangelson approximation[29] in the (p,α) case

$$\begin{aligned} V(\vec{r},\vec{r}_{12},\vec{r}_{123}) &\approx V^{(1)}(\vec{r})V^{(2)}(\vec{r}_{12},\vec{r}_{123}) \\ &= 3U_0 \exp(-\beta^2 r^2)\{\tfrac{2}{3}\exp[-\beta^2(\tfrac{1}{4}r_{12}^2 + \tfrac{1}{9}r_{123}^2)] + \tfrac{1}{3}\exp[-\beta^2(\tfrac{4}{9}r_{123}^2)]\} \end{aligned} \tag{15}$$

and in the Glendenning approximation,

$$V(\vec{r},\vec{r}_{12},\vec{r}_{123}) \approx V^{(1)}(r) = 3U_0 \exp(-\beta^2 r^2) \,. \tag{16}$$

The space part of the three-nucleon wave function is given as

$$\varphi_x(\vec{r}_1,\vec{r}_2,\vec{r}_3)^{\rho L}_{M_L} = \{[\varphi(\vec{r}_1)^{\rho_1} \times \varphi(\vec{r}_2)^{\rho_2}]^{\rho_{12} L_{12}} \times \varphi(\vec{r}_3)^{\rho_3}\}^{\rho L}_{M_L} \,, \tag{17}$$

with single-particle wave functions

$$\varphi(\vec{r}_i)^{\rho_i} = \frac{1}{r_i} u(r_i)_{n_i l_i j_i} Y^{l_i}_{m_i}(\hat{\vec{r}}_i)$$

which are calculated in a Woods-Saxon potential. In order to transform this wave function (17) to the new coordinates, we expand the single-particle wave functions $\varphi(\vec{r}_i)^{\rho_i}$ in terms of harmonic oscillator wave functions with the harmonic oscillator constant ν. The expansion coefficients are denoted by a_{p_i}, where p_i is the radial quantum number of the corresponding harmonic oscillator wave function. We then can transform the three-nucleon wave function to the above-mentioned coordinates using the generalized Talmi-Moshinsky brackets $\langle n_1 l_1 n_2 l_2 : \lambda \,|\, \mu_1 \mu_2 \,|\, NLnl : \lambda \rangle$.[30]

Inserting $\varphi_x(\vec{R},\vec{r}_{12},\vec{r}_{123})$, $V(\vec{r},\vec{r}_{12},\vec{r}_{123})$, and $\varphi_\alpha(\vec{r},\vec{r}_{12},\vec{r}_{123})$ into (11), the form factor split up into three terms, each depending on $\vec{R}$, $\vec{r}$, and $(\vec{r}_{12},\vec{r}_{123})$, respectively. Integrating now over the internal coordinates $\vec{r}_{12}$ and $\vec{r}_{123}$ we obtain

$$\begin{aligned} F^{\rho L}_{M_L}(\vec{R},\vec{r}) = D(\vec{r}) \sum_{\substack{N' N'_{12} \\ n' n''}} \sum_{p_1 p_2 p_3} & a_{p_1} a_{p_2} a_{p_3} \langle p_1 l_1 p_2 l_2 : L_{12} \,|\, \mu\mu \,|\, N'_{12} L_{12} n' 0 : L_{12} \rangle \\ & \times \langle N'_{12} L_{12} p_3 l_3 : L \,|\, 2\mu\mu \,|\, N' L n'' 0 : L \rangle I_{n' n''} \Phi^{N' L}_M(\vec{R}) \end{aligned} \tag{18}$$

with the r-dependent finite range normalization factor

$$\begin{aligned} D^{(\mathrm{p},\alpha)}(\vec{r}) &= \varphi^{(1)}_\alpha(\vec{r}) V^{(1)}(\vec{r}) \\ &= 3U_0 \left[\frac{3\nu_\alpha}{4\pi}\right]^{3/4} \exp[-r^2(\beta^2 + \tfrac{3}{8}\nu_\alpha)] \,. \end{aligned} \tag{19}$$

The radial form factor $\Phi^{N' L}_M(\vec{R})$ is the spherical harmonic oscillator function

$$\Phi^{N' L}_M(\vec{R}) = \frac{1}{R} H_{N' L}(3\nu R^2) Y^L_M(\hat{R}) \,. \tag{20}$$

The overlap $I_{n' n''}$ is the integral over the internal coordinates $\vec{r}_{12}$ and $\vec{r}_{123}$. Using the Chant-Mangelson approximation for the potential (15) we get

$$\begin{aligned} I_{n' n''} = (4\nu_\alpha \nu)^{3/2} & \left[\frac{(2n'+1)!!(2n''+1)!!}{n'! n''! 2^{n'} 2^{n''}}\right]^{1/2} \\ \times \Bigg\{ & \frac{2\left[\dfrac{\nu_\alpha + \beta^2 - \nu}{\nu_\alpha + \beta^2 + \nu}\right]^{n'} \left[\dfrac{\nu_\alpha + \frac{1}{3}\beta^2 - \nu}{\nu_\alpha + \frac{1}{3}\beta^2 + \nu}\right]^{n''}}{3[(\nu_\alpha + \beta^2 + \nu)(\nu_\alpha + \frac{1}{3}\beta^2 + \nu)]^{3/2}} \\ & + \frac{\left[\dfrac{\nu_\alpha - \nu}{\nu_\alpha + \nu}\right]^{n'} \left[\dfrac{\nu_\alpha + \frac{4}{3}\beta^2 - \nu}{\nu_\alpha + \frac{4}{3}\beta^2 + \nu}\right]^{n''}}{3[(\nu_\alpha + \nu)(\nu_\alpha + \frac{4}{3}\beta^2 + \nu)]^{3/2}} \Bigg\} \,. \end{aligned} \tag{21}$$

In the case of the Glendenning approximation (16) we obtain

$$\begin{aligned} I_{n' n''} = (4\nu_\alpha \nu)^{3/2} & \left[\frac{(2n'+1)!!(2n''+1)!!}{n'! n''! 2^{n'} 2^{n''}}\right]^{1/2} \\ & \times (\nu_\alpha + \nu)^{-3} \left[\frac{\nu_\alpha - \nu}{\nu_\alpha + \nu}\right]^{n'+n''} \,. \end{aligned} \tag{22}$$

In the zero-range approximation the normalization factor (19) is given as

$$D^{(\mathrm{p},\alpha)}(\vec{r}) = \varphi^{(1)}_\alpha(\vec{r}) V^{(1)}(\vec{r}) \approx D^{(\mathrm{p},\alpha)}_0 \delta(\vec{r}) \,. \tag{23}$$

The value of $D^{(\mathrm{p},\alpha)}_0$ can be calculated by

$$\begin{aligned} D^{(\mathrm{p},\alpha)}_0 &= \int d\vec{r}\, \varphi^{(1)}_\alpha(\vec{r}) V^{(1)}(\vec{r}) \\ &= 3U_0 \frac{(\frac{3}{4}\pi\nu_\alpha)^{3/4}}{(\frac{3}{8}\nu_\alpha + \beta^2)^{3/2}} \,. \end{aligned} \tag{24}$$

With the values for U_0, ν_α, and β given already, we obtain

$$(D_0^{(\mathrm{p},\alpha)})^2=2.56\times10^5\ \mathrm{MeV^2\,fm^3}\ . \tag{25}$$

In the projectile form factor (23) we use a Gaussian nucleon-nucleon interaction and a Gaussian α-particle wave function. With the same assumptions, but with an rms radius of the α particle $\langle r^2\rangle^{1/2}=1.45$ fm, Kunz *et al.*[10] obtain a theoretical value $D_0^{(\mathrm{p},\alpha)}=436\ \mathrm{MeV\,fm^{3/2}}$. The same projectile form factor is needed in (^{3}He,α) reactions. For this type of reaction Shepard *et al.*[31] give $D_0^{(^3\mathrm{He},\alpha)}=275$–$500\ \mathrm{MeV\,fm^{3/2}}$. The different theoretical values are due to varying assumptions for the nucleon-nucleon interaction and α-particle wave function.

C. Transition amplitude with a cluster form factor

In the cluster approximation the expressions (4)—(6) are replaced by

$$\hat{V}=V_{\mathrm{t,p}}^{(1)}(\vec{\mathrm{r}})\ , \tag{26}$$

$$\hat{\psi}_\alpha^a(\xi_\mathrm{t},\xi_\mathrm{p})=\varphi_\alpha^{(1)}(\vec{\mathrm{r}})_{M_\alpha=0}^{L_\alpha=0}\chi_\alpha^a(\mathrm{t,p})_{M_{S_\alpha}=N_\alpha=0}^{S_\alpha=T_\alpha=0}\ , \tag{27}$$

$$\psi_A^a(\xi_A)_{M_AN_A}^{J_AT_A}=(\tfrac{A}{3})^{-(1/2)}\sum_{JJ_B}\sum_{TT_B}\sum_{LS}\hat{S}_{AB}^{1/2}(LSJT)[\psi_B^a(\xi_B)^{J_BT_B}\times\psi_\mathrm{t}(\xi_\mathrm{t})^{LSJT}]_{M_AN_A}^{J_AT_A}\ , \tag{28}$$

with the wave functions given in the $LSJT$ representation and the cluster space, spin, and isospin coordinates $\xi_t=(\vec{\mathrm{R}},\sigma_\mathrm{t},\tau_\mathrm{t})$. Performing the spin algebra we get for the transition matrix

$$\begin{aligned}T_{(\mathrm{p},\alpha)}^{\mathrm{DWBA}}(A,B)=(\tfrac{4}{3})^{1/2}&\sum_{JM}\langle J_BM_BJM\mid J_AM_A\rangle\langle T_BN_B\tfrac{1}{2}(-\tfrac{1}{2})\mid T_AN_A\rangle\\&\times\sum_L\langle L(M+M_\mathrm{p})\tfrac{1}{2}(-M_\mathrm{p})\mid JM\rangle\langle\tfrac{1}{2}M_\mathrm{p}\tfrac{1}{2}(-M_\mathrm{p})\mid 00\rangle\langle\tfrac{1}{2}\tfrac{1}{2}\tfrac{1}{2}(-\tfrac{1}{2})\mid 00\rangle\\&\times\hat{S}_{AB}^{1/2}(L\tfrac{1}{2}J\tfrac{1}{2})\int\int d\vec{\mathrm{R}}\,d\vec{\mathrm{r}}\,\chi^{(-)*}(\vec{\mathrm{k}}_\alpha,\vec{\mathrm{r}}_{\alpha B})\hat{F}_{M_L}^{LJ}(\vec{\mathrm{R}},\vec{\mathrm{r}})\chi^{(+)}(\vec{\mathrm{k}}_\mathrm{p},\vec{\mathrm{p}}_{\mathrm{p}A})\ ,\end{aligned} \tag{29}$$

where the form factor $\hat{F}_{M_L}^{LJ}(\vec{\mathrm{R}},\vec{\mathrm{r}})$ is given as

$$\begin{aligned}\hat{F}_{M_L}^{LJ}(\vec{\mathrm{R}},\vec{\mathrm{r}})&=\langle\varphi_\alpha^{(1)}(\vec{\mathrm{r}})_0^0\mid V_{\mathrm{t,p}}^{(1)}(\vec{\mathrm{r}})\mid\varphi_\mathrm{t}(\vec{\mathrm{R}})_{M_L}^{LJ}\rangle\\&=D(\vec{\mathrm{r}})\varphi_\mathrm{t}(\vec{\mathrm{R}})_{M_L}^{LJ}\ ,\end{aligned} \tag{30}$$

with the radial wave function $\varphi_\mathrm{t}(\vec{\mathrm{R}})_{M_L}^{LJ}$ calculated in a Woods-Saxon potential between B and t.

The cluster ansatz for the form factor (30) can be founded in the microscopic formulation when one makes the following assumptions:

(i) a harmonic oscillator potential for the single-nucleon states in the microscopic model, i.e., $a_{p_i}\to\delta_{p_i,n_i}$ ($i=1,2,3$) in (18);

(ii) the Glendenning approximation (16); and

(iii) the same harmonic oscillator constants for the target nucleus and the α particle, i.e., $\nu=\nu_\alpha$.

With these assumptions one finds that the microscopic form factor (18) factorizes into a structure part and a dynamical part

$$\begin{aligned}F_{M_L}^{\rho L}(\vec{\mathrm{R}},\vec{\mathrm{r}})=&\langle n_1l_1n_2l_2{:}L_{12}\mid\mu\mu\mid N_{12}L_{12}00{:}L_{12}\rangle\\&\times\langle N_{12}L_{12}n_3l_3{:}L\mid 2\mu\mu\mid NL\,00{:}L\rangle D(\vec{\mathrm{r}})\Phi_{M_L}^{NL}(\vec{\mathrm{R}})\ .\end{aligned} \tag{31}$$

The radial quantum number is now restricted to its maximum value N, which is given by the conservation of oscillator quanta in the Talmi-Moshinsky transformation

$$Q\equiv2N+L=\sum_{i=1}^{3}(2n_i+l_i)\equiv\sum_{i=1}^{3}qi\ . \tag{32}$$

D. Spectroscopic factors

The inversion of the relation (6) gives for the spectroscopic amplitude in the microscopic description

$$S_{AB}^{1/2}(\rho JT)=(\tfrac{A}{3})^{1/2}\langle[\psi_B^a(\xi_B)^{J_BT_B}\times\psi_x^a(\xi_1,\xi_2,\xi_3)^{\rho JT}]_{M_AN_A}^{J_AT_A}\mid\psi_A^a(\xi_A)_{M_AN_A}^{J_AT_A}\rangle\ . \tag{33}$$

In order to use the results of shell-model calculations we have to transform the nuclear wave functions $\psi(\xi)$ to shell-model wave functions $\Psi(\zeta)$. This can be accomplished by using the cluster ansatz for the microscopic form factor described in Sec. II C. We obtain in analogy to Ref. 14

$$S_{AB}^{1/2}(\rho JT)=\binom{A}{3}^{1/2}\left[\frac{A}{A-3}\right]^{Q/2}\langle[\Psi_B^a(\zeta_B)^{J_BT_B}\times\Psi_x^a(\zeta_1,\zeta_2,\zeta_3)^{\rho JT}]_{M_AN_A}^{J_AT_A}\mid\Psi_A^a(\zeta_A)_{M_AN_A}^{J_AT_A}\rangle\ . \tag{34}$$

Next we expand the wave functions of the target nucleus A and residual nucleus B using pure shell-model configurations

$$\begin{aligned}\mid\Psi_A^{AT_A}\rangle&=\sum_{\rho_A}a_{\rho_A}\mid\rho_AJ_AT_A\rangle\ ,\\ \mid\Psi_B^{BT_B}\rangle&=\sum_{\rho_B}b_{\rho_B}\mid\rho_BJ_BT_B\rangle\ ,\\ \mid\Psi^{\rho JT}\rangle&=\mid\rho JT\rangle\ ,\end{aligned}\tag{35}$$

where the ρ's characterize the different configurations. The coefficients a_{ρ_A} and b_{ρ_B} denote the amplitudes of the different shell-model configurations of the target nucleus A and residual nucleus B, respectively. Then we obtain for the spectroscopic amplitude

$$S_{AB}^{1/2}(\rho JT)=\binom{A}{3}^{1/2}\left[\frac{A}{A-3}\right]^{Q/2}\times\sum_{\rho_A\rho_B}a_{\rho_A}b_{\rho_B}S_{\rho_A\rho_B}^{1/2}(\rho JT)\ , \tag{36}$$

where the $S_{\rho_A\rho_B}^{1/2}(\rho JT)$ are the spectroscopic amplitudes for the pure shell model configurations.

There are two methods to obtain the transition amplitude in a semimicroscopic model. In the first one[12,13] the transition amplitude (10) can be determined by inserting the form factor in the cluster approximation (31). In the second one, applicable to light nuclei with $A\leq 40$, the SU(3) cluster model can be used which will be described in the following.

In this model we obtain for the spectroscopic amplitude, by inverting (28) and using the transformation to shell-model wave functions,

$$\hat{S}_{AB}^{1/2}(LSJT)=\binom{A}{3}^{1/2}\left[\frac{A}{A-3}\right]^{Q/2}\langle[\Psi_B^a(\zeta_B)^{J_BT_B}\times\Psi_t(\zeta_t)^{LSJT}]_{M_AN_A}^{J_AT_A}\mid\Psi_A^a(\zeta_A)_{M_AN_A}^{J_AT_A}\rangle\ . \tag{37}$$

Now we apply the coefficient of fractional parentage technique to $\Psi_A(\zeta_A)_{M_AN_A}^{J_AT_A}$ and obtain

$$\hat{S}_{AB}^{1/2}(LSJT)=\binom{A}{3}^{1/2}\left[\frac{A}{A-3}\right]^{Q/2}\sum_{\beta}\langle\Psi_B\Psi_\beta\mid\}\Psi_A\rangle\langle\Psi_t(\zeta_t)_{MN}^{LSJT}\mid\Psi_\beta(\zeta_1,\zeta_2,\zeta_3)\rangle\ , \tag{38}$$

where the $\Psi_B(\zeta_1,\zeta_2,\zeta_3)$ form a complete set of three-particle shell-model wave functions with β being all the quantum numbers necessary to specify the states.

In order to calculate the overlap

$$\langle\Psi_t(\zeta_t)_{MN}^{LSJT}\mid\Psi_\beta(\zeta_1,\zeta_2,\zeta_3)\rangle$$

we have to make the following assumptions about the triton wave function.

(i) The three-particle cluster is transferred in a fully spatially symmetric $0s$ state.

(ii) The center-of-mass motion of the triton cluster with respect to the center of the shell-model potential is described by a harmonic oscillator wave function.

(iii) The harmonic oscillator size parameters of the internal and the center-of-mass motion are the same.

Then the three-particle shell-model wave functions $\Psi_\beta(\zeta_1,\zeta_2,\zeta_3)$ are assumed to be specified by wave functions in the SU(3) representation

$$\mid\Psi_\beta(\zeta_1,\zeta_2,\zeta_3)\rangle=\mid\Psi_{[f](\lambda\mu)qLSJTMN}^{SU(3)}(\zeta_1,\zeta_2,\zeta_3)\rangle\ , \tag{39}$$

with $[f]$ being the space symmetry quantum numbers, $(\lambda\mu)$ the Elliot SU(3) quantum numbers, and q all the additional quantum numbers needed to characterize the SU(3) state. With these assumptions we obtain[14,16]

$$\hat{S}_{AB}^{1/2}(LSJT)=\binom{A}{3}^{1/2}\left[\frac{A}{A-3}\right]^{Q/2}\langle\Psi_B\Psi_{\hat{\beta}}^{SU(3)}\mid\}\Psi_A\rangle G \tag{40}$$

with the overlap factor

$$\begin{aligned}G&=\langle\Psi_t(\zeta_t)_{MN}^{LSJT}\mid\Psi_{\hat{\beta}}^{SU(3)}(\zeta_1,\zeta_2,\zeta_3)\\&=\left[\frac{Q!}{3^Qq_1!q_2!q_3!}\right]^{1/2}\end{aligned}\tag{41}$$

if the three transferred particles are taken from the same oscillator shell. The oscillator quantum numbers Q and q_i are defined by (32). The SU(3) wave function $\Psi_{\hat{\beta}}^{SU(3)}$ in the $(Q0)$ representation is given by

$$\Psi_{\hat{\beta}}^{SU(3)}=\Psi_{[3](Q0)L\,1/2J\,1/2MN}^{SU(3)}(\zeta_1,\zeta_2,\zeta_3) \tag{42}$$

and is in this case independent of the additional quantum

numbers q introduced in (39). In order to calculate the coefficient of fractional parentage $\langle \Psi_B \Psi_{\hat{\beta}}^{SU(3)} | \} \Psi_A \rangle$ we make the following expansions using pure shell-model functions in analogy to (35):

$$|\Psi_A^{J_A T_A}\rangle = \sum_{\rho_A} q_{\rho_A} |\rho_A J_A T_A\rangle ,$$
$$|\Psi_B^{J_B T_B}\rangle = \sum_{\rho_S} b_{\rho_B} |\rho_B J_B T_B\rangle , \quad (43)$$
$$|\Psi_{\hat{\beta}}^{SU(3)}\rangle = \sum_{\rho} c_\rho^{JT} |\rho JT\rangle .$$

Inserting (43) into (40) and using (36), the cluster spectroscopic amplitude can be expressed in terms of the microscopic spectroscopic amplitudes and of the coefficients c_ρ^{JT}

$$\hat{S}_{AB}^{1/2}(LSJT) = G \sum_\rho c_\rho^{JT} S_{AB}^{1/2}(JT) , \quad (44)$$

with

$$c_\rho^{JT} = \langle \Psi_{\hat{\beta}}^{SU(3)} | \rho JT \rangle . \quad (45)$$

For reactions between nuclei of the same oscillator shell this overlap integral (45) is independent of the quantum numbers of the target nucleus A and the residual nucleus B.

III. EXPERIMENTAL PROCEDURE

The (p,α) experiments on ^{27}Al were carried out at four energies between 20 and 45 MeV. The proton beam with an energy of 20 and 24 MeV was provided by the MP-tandem accelerator of the Max-Planck-Institut (MPI), Heidelberg. The target consisted of a self-supporting aluminum foil of a thickness of about 90 μg/cm^2. The absolute cross section derived from this experiment is in fair agreement with the ^{24}Mg(α,p)^{27}Al data at the 28.8 MeV α energy of August *et al.*[32] The error in the absolute cross section is estimated to be less than 15%. The outgoing α particles were detected using nuclear track plates positioned in the focal plane of the Heidelberg multigap magnetic spectrograph. The gaps cover the angular range between 5.5° and 172.5° in steps of 3.5 degrees at angles less than 90° and in steps of 7 degrees at backward angles. The good energy resolution of about 30 keV full width at half maximum of forward angles and the broad energy range of the spectrograph allowed the evaluation of transitions to states in ^{24}Mg up to an excitation energy of 9 MeV. Figure 2(a) shows a typical spectrum of the ^{27}Al(p,α)^{24}Mg reactions at $E_p = 20$ MeV and $\theta_{lab} = 36°$.

The experiments at $E_p = 30.5$ and 45 MeV were performed using the proton beam of the isochronous cyclotron JULIC of the Kernforschungsanlage KFA-Jülich. The target consisted of a rolled aluminum foil of a thickness of about 600 μg/cm^2. The outgoing α particles were detected by up to five Si-surface barrier detectors placed in a 1 m diam scattering chamber. The scattered protons were detected at an angle of 30° using a Ge(Li) detector positioned outside of the scattering chamber. These count rates were used to monitor the beam and to correct for in-

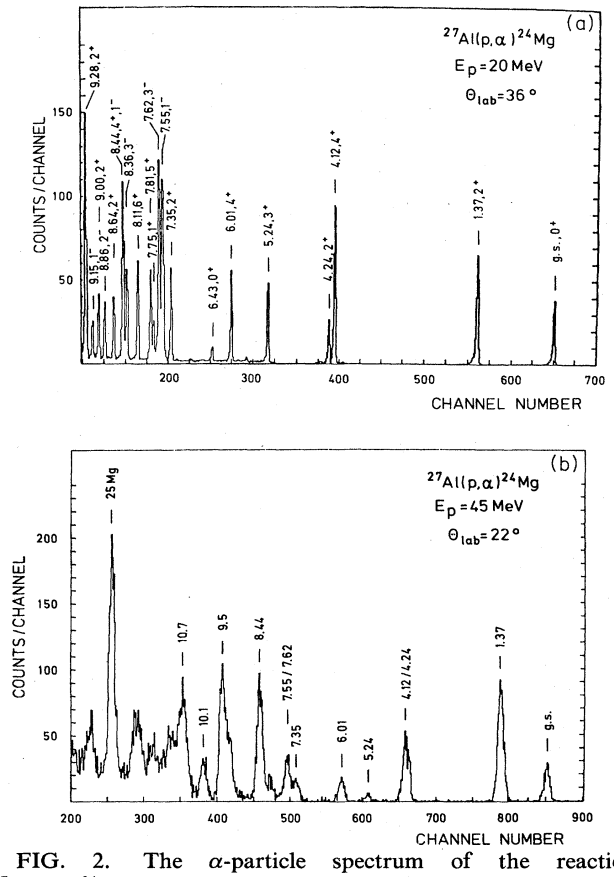

FIG. 2. The α-particle spectrum of the reaction ^{27}Al(p,α)^{24}Mg (a) at $E_p = 20$ MeV and for $\theta = 36°$; (b) at $E_p = 45$ MeV and for $\theta = 22°$.

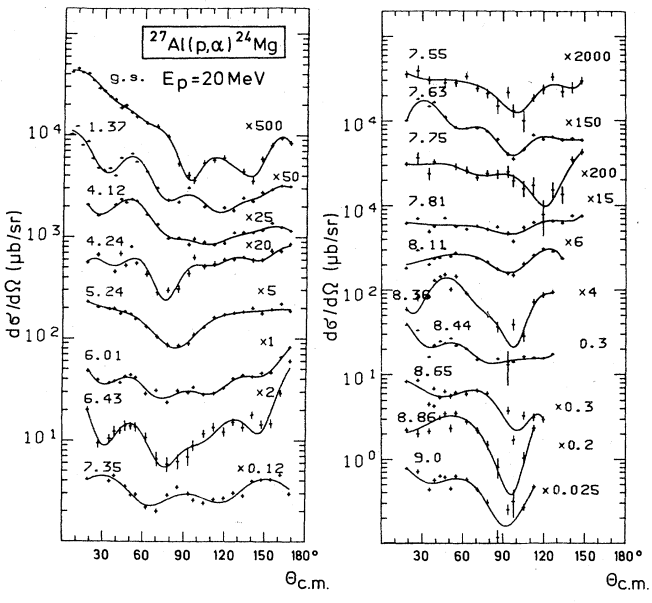

FIG. 3. Angular distributions for the reaction ^{27}Al(p,α)^{24}Mg at $E_p = 20$ MeV leading to the ground state and to excited states up to $E_x = 9$ MeV. Solid lines are Legendre polynomial fits.

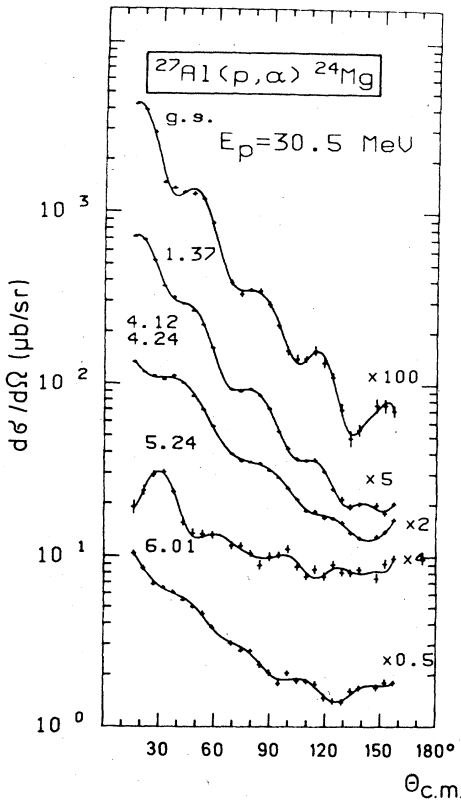

FIG. 4. Same as Fig. 3, but at $E_p=30.5$ MeV leading to the ground state and to excited states up to $E_x=6$ MeV. Solid lines are Legendre polynomial fits.

homogeneities in the target. The detector signals were amplified and registered by means of standard nuclear electronics. Due to the small cross section of the reaction an unanalyzed beam of about 1 μA was used. This resulted, combined with the target thickness, in an energy resolution of about 250 keV full width at half maximum. At the proton energy of 30.5 MeV the ^{27}Al(p,α)^{24}Mg reaction was measured in steps of 5 degrees at angles between 15° and 150° and at $E_p=45$ MeV in the range between 12° and 85°. Figure 2(b) shows a spectrum for this reaction at $E_p=45$ MeV and $\theta_{lab}=22°$.

The angular distributions for the reaction ^{27}Al(p,α)^{24}Mg are shown in Figs. 3 and 4. The errors indicated are only the statistical errors, the solid lines correspond to Legendre-polynomial fits to the data. At 20 MeV proton energy 18 transitions to excited states in ^{24}Mg have been analyzed separately. The worse energy resolution in the experiments using the scattering chamber only allowed the analysis of five transitions at 30.5 and 45 MeV proton energy, respectively. For these energies the doublet at 4.12/4.24 MeV excitation energy could not be resolved.

IV. DWBA CALCULATIONS

A. Optical potentials

The differential cross sections for the ground state transitions at $E_p=24$, 30.5, 35, and 45 MeV and for the transitions to excited states at $E_p=30.5$ and 45 MeV have been calculated using the DWBA. In order to achieve a description of the (p,α) reaction without adjusting any parameters to the reaction itself, we first started a search procedure for the optical potential parameters using the computer code GOMFIL.[33] This program allows one to fit elastic data with energy-dependent optical potentials.

The experimental data for the proton elastic scattering on ^{27}Al are taken from the work of Sandhu.[34] To fit these data in the energy range between 24.5 and 61.2 MeV we started with the optical model parameters of the global potential of Becchetti and Greenlees.[35] Then the geometry parameters have been kept fixed and only the depth of the potential well and its energy dependence have been varied. The result of this procedure is shown together with the experimental data in Fig. 5(a). The resulting parameter set is listed in Table I and labeled with Pot *P*.

For the elastic scattering of α particles on ^{24}Mg, experimental data at 22.2, 28, 42, and 50.1 MeV have been used.[36–39] Since an α energy of 50 MeV corresponds quite well to the energy of the α particles in the ^{27}Al(p,α)^{24}Mg reaction at a proton energy of 45 MeV, first of all a fit with an energy-independent potential was performed at the energy of 50.1 MeV. The parameters of this potential are listed in Table I as Pot *A*1 and the resulting fit to the elastic data is shown in Fig. 5(b) as a dashed line.

Starting with the parameters of this potential we tried to fit all the data in the energy range between 22.2 and 50.1 MeV. Several families of α-optical potentials have been found which give similarly fair fits to the elastic

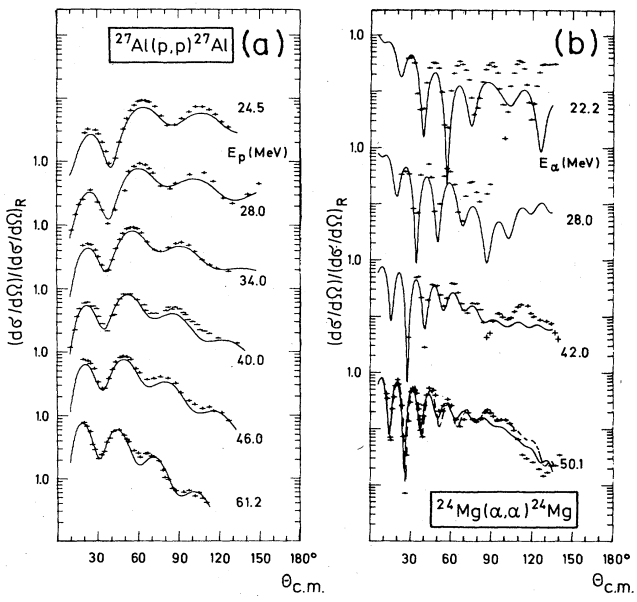

FIG. 5. Differential cross sections for elastic scattering processes together with optical potential fits. (a) The reaction ^{27}Al(p,p)^{27}Al at E_p between 24.5 and 61.2 MeV. The optical potential parameters are given in Table I as Pot *P*. (b) The reaction ^{24}Mg(α,α)^{24}Mg at E_α between 22.2 and 50.1 MeV. Solid lines and the dashed line are the result of using optical potentials Pot *A*2 and Pot *A*1 of Table I, respectively.

TABLE I. Optical-model parameters used in the DWBA calculations. For the optical potentials the definition of Perey and Perey (Ref. 62) is used. The energy dependence is signed by $|V(E)| = |V| + kE_{\text{lab}}$.

	Type	$\|V_R\|$/(MeV)	k_R	r_{0R}/(fm)	a_R/(fm)	$\|V_I\|$/(MeV)	k_I	r_{0I}/(fm)	a_I/(fm)	r_{0C}/(fm)
Pot *P*	Vol.	55.61	−0.331	1.17	0.75	9.48	+0.04	1.32	0.51	1.2
	so	6.63		1.01	0.75					
Pot *A*1	Vol.	202.7		1.32	0.565	36.49		1.414	0.58	1.3
Pot *A*2	Vol.	274.1	−0.936	1.225	0.65	5.68	+0.976	1.236	0.72	1.35

data. But only with one set of parameters was a description of the (p,α) reaction possible. The parameters of this energy-dependent α potential are given in Table I, labeled with Pot *A*2. The fits to the elastic data are shown in Fig. 5(b) as solid lines. For the lower energy the agreement is unsatisfactory. This may be caused by the assumption of a Woods-Saxon potential which is inadequate to reproduce α-scattering data at low energies. This has also been found by Michel *et al.*[40] for the elastic α-^{16}O scattering.

B. Form factors

To calculate the microscopic form factors, the single-particle wave functions of the transferred $d_{5/2}$, $s_{1/2}$, and $d_{3/2}$ nucleons are required. The computer code BOUND (Ref. 41) allows one to calculate these wave functions in a Woods-Saxon potential, the binding energy of the particles, and the expansions in a series of harmonic oscillator wave functions. For our calculations two parameter sets of single-particle potentials have been used, listed in Table II as Pot 1 and Pot 2. They are taken from the systematics of Bear and Hodgson[42] and of Malaguti and Hodgson.[43] The depth of the potential well was determined from the separation energy of the nucleons. It was assumed to be $S_N = \frac{1}{3}(S_t + B_t)$, with S_t being the separation energy of the triton cluster and B_t the triton binding energy. The width of the harmonic oscillator is given by $\nu = (0.9A^{1/3} + 0.7)^{-1}$ fm^{-2}.[44]

The microscopic form factor Eq. (18) was calculated with these single-particle wave functions by the aid of the codes FORM (Ref. 45) in zero-range approximation and FFR (Ref. 46) in finite-range formulation. In the zero-range calculations the Glendenning approximation [Eq. (22)] is used and in the finite-range calculations the Chant-Mangelson approximation [Eq. (21)] is used. The resulting microscopic form factors $F^{\rho L}_{M_L}(\vec{R},\vec{r})$ are multiplied with the spectroscopic amplitudes $S^{1/2}_{AB}(\rho JT)$ and with the factor $g(\rho)$, and then summed up coherently over ρ [see Eq. (10)]. Since the shell-model spectroscopic amplitudes are given in *jj* coupling, a transformation from *jj* to *LS* coupling has to be performed prior to the multiplication. Then we obtain the weighted microscopic form factor $f^L_{M_L}(\vec{R})$,

$$D(\vec{r}) f^L_{M_L}(\vec{R}) = \sqrt{2}\langle T_B N_B TN \mid T_A N_A \rangle \sum_{\rho} \sum_{L_{12} S_{12}} (-1)^{T_{12}} \delta_{S_{12}+T_{12},1} \begin{Bmatrix} l_1 & \frac{1}{2} & j_1 \\ l_2 & \frac{1}{2} & j_2 \\ L_{12} & S_{12} & J_{12} \end{Bmatrix} \begin{Bmatrix} L_{12} & S_{12} & J_{12} \\ l_3 & \frac{1}{2} & j_3 \\ L & \frac{1}{2} & J \end{Bmatrix}$$

$$\times g(\rho) S^{1/2}_{AB}(\rho JT) F^{\rho_L}_{M_L}(\vec{R},\vec{r}) \, . \tag{46}$$

Due to the difference between the sum of the separation energies of the three nucleons in their respective single-particle states and the separation energy for a triton, the microscopic form factor does not have the correct asymptotic behavior. As usual, we replace it in the external region by the tail of the triton cluster form factor which is calculated for the separation energy S_t. The parameter sets of the Woods-Saxon potential needed for the smooth joining of exterior and interior form factors are listed in Table II as Pot 1*a* and Pot 2*a*, respectively. In this way, so-called hybrid form factors are obtained using the bound-state potentials Pot 1/1*a* or Pot 2/2*a*. The point of junction is taken as the point where the logarithmic derivations of the two functions are equal. To obtain a comparable expression to the weighted microscopic form factor [Eq. (46)], the cluster form factor [Eq. (30)] likewise is multiplied with the cluster spectroscopic amplitude giving the weighted cluster form factor $\hat{f}^{LJ}_{M_L}(\vec{R})$,

$$D(\vec{r}) \hat{f}^{J}_{M_L}(\vec{R}) = \sqrt{2}\langle T_B N_B TN \mid T_A N_A \rangle$$

$$\times \hat{S}^{1/2}_{AB}(LSJT) \hat{F}_{M_L}(\vec{R},\vec{r}) \, . \tag{47}$$

TABLE II. Woods-Saxon potentials for the bound states of the single particles (Pot 1, 2) and the triton cluster (Pot 1*a*, 2*a*). The potential depth V was calculated from the given separation energy.

	r_0/(fm)	a/(fm)	V_{LS}/(MeV)	r_{LS}/(fm)	a_{LS}/(fm)
Pot 1	1.236	0.62	7	1.236	0.65
Pot 1*a*	1.05	0.55			
Pot 2	1.35	0.52	5	1.10	0.65
Pot 2*a*	1.1	0.55			

Since both the microscopic and the SU(3) cluster spectroscopic amplitudes are based on the same shell-model calculation, the absolute values of both the weighted microscopic and cluster form factors are similar within 10% to each other in the region of the nuclear surface.

C. Spectroscopic amplitudes

The three-nucleon transfer spectroscopic amplitude as given by Eq. (36) is proportional to the reduced matrix element of the transferred group between initial and final states[47]

$$S_{AB}^{1/2}(\rho JT)=\binom{A}{3}^{1/2}\left[\frac{A}{A-3}\right]^{Q/2}\sum_{\rho_A\rho_B} a_{\rho_A} b_{\rho_B} S_{\rho_A\rho_B}^{1/2}(\rho JT)$$
$$=\left[\frac{A}{A-3}\right]^{Q/2}\left[\frac{1}{(2J_A+1)(2T_A+1)}\right]^{1/2}\langle (sd)^8_{J_BT_B}|||\mathcal{O}(sd)^3_{\rho JT}|||(sd)^{11}_{J_A=5/2\ T_A=1/2}\rangle\ , \tag{48}$$

where the triple-reduced matrix elements of the three-nucleon creation operator $\mathcal{O}(sd)^3_{\rho JT}$ reduced both in ordinary and isospin spaces are calculated between the (J_BT_B) final states in ^{24}Mg and the $(\frac{5}{2}\frac{1}{2})$ ground state of ^{27}Al for each of the created $(sd)^3_{\rho JT}$ components. These matrix elements were calculated by Chung[48] with the wave functions of Chung and Wildenthal.[49] In Table III the values of the calculated matrix elements are given for the ground state transition to ^{24}Mg. As one can see, the transition strength of the three seniority-one components contains about 50% of the total transition strength.

The SU(3) cluster spectroscopic amplitude is based on the same shell-model wave function[49] as the microscopic one and is given by Eq. (44). Together with Eq. (48) it can be written as

$$\hat{S}_{AB}^{1/2}(LSJT)=\left[\frac{A}{A-3}\right]^{Q/2} GP^{JT}\ , \tag{49}$$

with the parentage amplitude for a given (JT) transfer between the initial state $(J_A=\frac{5}{2},\ T_A=\frac{1}{2})$ and the final state (J_BT_B),

$$P^{JT}=\left[\frac{1}{(2J_A+1)(2T_A+1)}\right]^{1/2}\sum_{\rho} c_\rho^{JT}\langle (sd)^8_{J_BT_B}|||\mathcal{O}(sd)^3_{\rho JT}|||(sd)^{11}_{J_A=5/2\ T_A=1/2}\rangle\ . \tag{50}$$

For the ^{27}Al(p,α)^{24}Mg reaction the numbers of oscillator quanta are given by $q_1=q_2=q_3=2$ and $Q=6$. Therefore, the G factor, Eq. (41), has the value $G=(\frac{10}{81})^{1/2}$. In order to get the coefficients c_ρ^{JT}, Eq. (45), the wave functions $\Psi_\beta^{SU(3)}$ have been calculated by Chung[48] in the leading $(\lambda\mu)=(60)$—representation of SU(3) by diagonalizing the quadrupole-quadrupole interaction[47,50] with an admixture of 0.1% of the Chung-Wildenthal interaction, whereas for $|\rho JT\rangle$ the three-particle configurations of ^{19}F are used. In Table IV the values of the parentage amplitudes P^{JT} calculated by Chung[48] are given for some (p,α) transitions to the residual nucleus ^{24}Mg. The second column lists the calculated excitation energies, the last column lists the sum over J of the squared amplitudes for each final state, which is a rough measure of the expected cross section.

D. Calculation of the differential cross section

As described in Sec. II, the microscopic form factor is separated in the variables $\vec{r}$ and $\vec{R}$, corresponding to the relative motion of the center of mass of the three

TABLE III. Reduced matrix elements $M=\langle (sd)^8_{00}|||\mathcal{O}(sd)^3_{\rho(5/2)(1/2)}|||(sd)^{11}_{(5/2)(1/2)}\rangle$. $(j_1)=d_{5/2}$; $(j_2)=s_{1/2}$; $(j_3)=d_{3/2}$.

Configuration ρ	Seniority ν	M	Configuration ρ	Seniority ν	M
$(j_3)^3$	3	0.0426	$(j_1j_2)_{31}(j_3)$	3	0.0712
$(j_2)(j_3)^2_{21}$	3	−0.0966	$(j_1)(j_2)^2_{01}$	1	−0.5430
$(j_2)(j_3)^2_{30}$	3	−0.0190	$(j_1)(j_2)^2_{10}$	3	0.2159
$(j_2)^2_{10}(j_3)$	3	−0.1186	$(j_1)^2_{10}(j_3)$	3	−0.0089
$(j_1)(j_3)^2_{01}$	1	−0.5434	$(j_1)^2_{21}(j_3)$	3	−0.0918
$(j_1)(j_3)^2_{10}$	3	−0.1087	$(j_1)^2_{30}(j_3)$	3	−0.0604
$(j_1)(j_3)^2_{21}$	3	0.0054	$(j_1)^2_{41}(j_3)$	3	−0.1510
$(j_1)(j_3)^2_{30}$	3	−0.0394	$(j_1)^2_{21}(j_2)$	3	0.0987
$(j_1j_2)_{20}(j_3)$	3	−0.0262	$(j_1)^2_{30}(j_2)$	3	−0.1524
$(j_1j_2)_{21}(j_3)$	3	−0.0902	$(j_1)^3$	1	−0.6607
$(j_1j_2)_{30}(j_3)$	3	−0.0791	$(j_1)^3$	3	−0.1327

TABLE IV. SU(3) parentage amplitudes $P^{JT}=(\frac{1}{12})^{1/2}\sum_{\rho} c_{\rho}^{JT}\langle (sd)^8_{J_B T_B}|||\mathcal{O}(sd)^3_{\rho JT}|||(sd)^{11}_{(5/2)(1/2)}\rangle$ and calculated excitation energies $E_{\rm cal}$ for the reaction ^{27}Al(p,α)^{24}Mg. (SUMSQ denotes the sum of the squared spectroscopic amplitudes.)

J_B	T_B	$E_{\rm cal}$ (MeV)	$S_{1/2}$	$D_{3/2}$	$D_{5/2}$	$G_{7/2}$	$G_{9/2}$	$I_{11/2}$	$I_{13/2}$	SUMSQ
0	0	g.s.			0.2622					0.0687
		7.421			−0.0115					0.0001
1	0	7.775		0.0293	0.0214	−0.0076				0.0014
2	0	1.564	0.0099	0.0213	−0.3188	−0.0761	−0.0706			0.1130
		4.117	0.0788	−0.0992	−0.0527	−0.0246	−0.0769			0.0253
		7.529	0.1773	0.0246	0.0965	0.0065	−0.0751			0.0470
		9.262	−0.1362	−0.0514	0.0423	0.0184	0.0597			0.0269
3	0	5.166	0.1389	−0.0585	−0.0366	−0.0865	−0.1000	−0.0330		0.0426
4	0	4.425		−0.0265	0.2822	0.0882	0.1658	−0.0459	−0.0319	0.1187
		5.893		−0.0019	−0.1918	−0.0931	−0.0790	0.0951	0.1027	0.0741
		8.795		0.0691	−0.3347	0.0118	0.0838	−0.0043	−0.0917	0.1324
5	0	7.904			0.0943	0.0566	0.0344	−0.0425	0.1006	0.0252
6	0	8.472				0.0232	0.1892	−0.0066	−0.0685	0.0411

transferred particles with the incoming particle and the core, respectively. Therefore, the differential cross sections can be calculated in finite-range formulation by the use of the DWBA code DWUCK V.[51] In zero-range approximation we have used the code DWUCK IV.[52] In both cases the total microscopic form factors $f^L_{M_L}(\vec{R})$ have been programmed externally. The cluster form factors $\hat{f}^{LJ}_{M_L}(\vec{R})$ were calculated in subroutines provided by the above DWBA codes.

The experimental cross section is related to the DWBA cross section calculated with DWUCK V by

$$\left[\frac{d\sigma}{d\Omega}\right]_{\rm exp}=\epsilon_{\rm FR}\left[\frac{d\sigma}{d\Omega}\right]_{\rm DWUCK\ V}. \tag{51}$$

Using the DWBA code DWUCK IV the experimental cross section is given by

$$\left[\frac{d\sigma}{d\Omega}\right]_{\rm exp}=\frac{\epsilon_{\rm ZR}}{(2s_{\rm p}+1)}\frac{D_0^2({\rm p},\alpha)}{10^4}\times\sum_J\frac{1}{(2J+1)}\left[\frac{d\sigma}{d\Omega}\right]^J_{\rm DWUCK\ IV}. \tag{52}$$

The normalization factors $\epsilon_{\rm FR}$ and $\epsilon_{\rm ZR}$ describe the deviations between experiment and theory in finite-range (FR) formulation and zero-range (ZR) approximation, respectively.

V. ANALYSIS AND DISCUSSION

A. Microscopic analysis of the ground state transition

In order to analyze the experimental data, we start with microscopic DWBA calculations of the ground state transition at four energies between $E_{\rm p}=24$ and 45 MeV. Using the hybrid form factors, as they are introduced in Sec. IV B, and the optical potentials Pot *P*, Pot *A*1, and Pot *A*2 (see Table I), several DWBA calculations in zero-range and finite-range approximation have been performed. Some results of calculated angular distributions are shown in Fig. 6 together with the experimental data. The data at $E_{\rm p}=35$ MeV are taken from the work of Brunner *et al.*[53] The normalization factors $\epsilon_{\rm FR}$ and $\epsilon_{\rm ZR}$ as defined by Eqs. (51) and (52) are listed in Table V.

In Fig. 6(a) the experimental data at 45 MeV are given together with some theoretical curves calculated with the energy-independent potential Pot *A*1. The curves are very similar to each other and give a fair fit to the data. The differences between the calculated angular distribution obtained in zero-range and finite-range approximation are small. But for the absolute normalization a factor of about 65 is needed in the zero-range calculations, whereas a normalization factor of about 200 has been found in the finite-range calculations. These values are in good agreement with the normalization constants given by Brunner *et al.*[54] The factor of 3 between the normalization of the zero-range and finite-range calculations is attributed to the more crude Glendenning approximation used in the zero-range calculations.

As has been shown in Sec. IV A, both the proton and the alpha elastic scattering can be described by an energy-dependent optical potential. Using these potentials (Pot *P*, Pot *A*2) we have calculated the ground state transitions at $E_{\rm p}=24$, 30.5, 35, and 45 MeV. In Fig. 6(b) the experimental data are compared with the results of zero-range calculations. The hybrid form factor used was calculated with the bound potential using the parameter set of Pot 2/2*a*.

Comparing the results obtained with the energy-

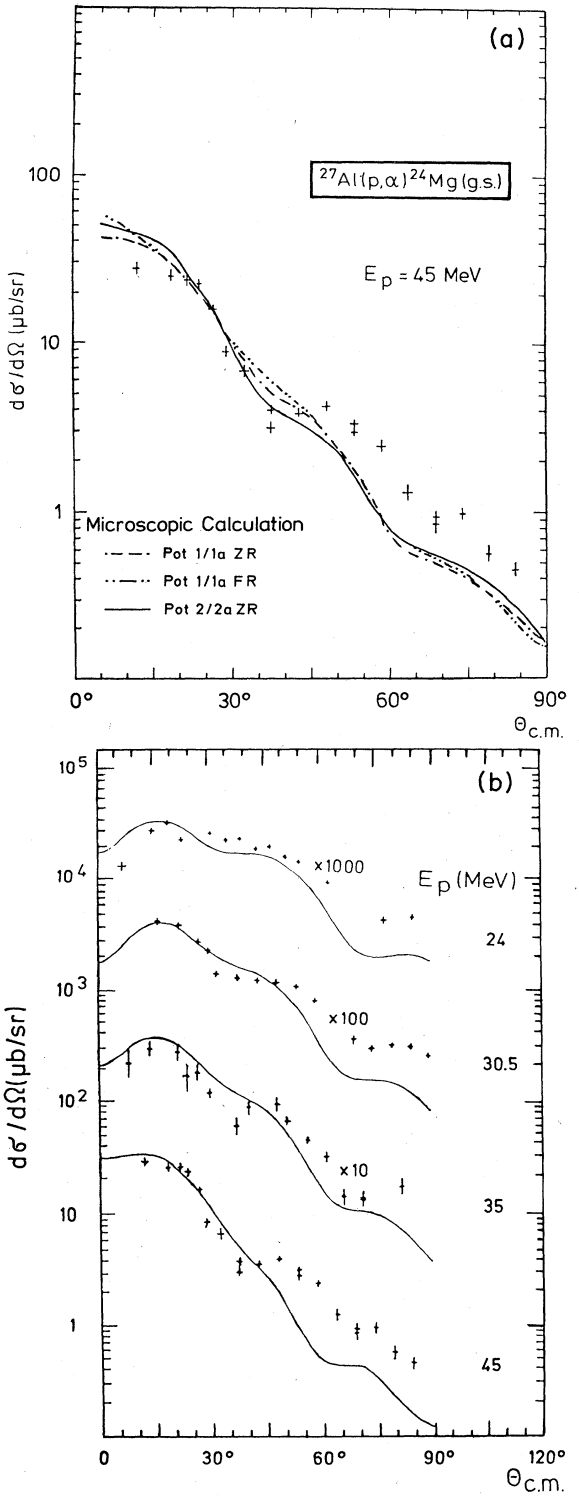

FIG. 6. Differential cross sections for the reaction ^{27}Al(p,α)^{24}Mg(g.s.) at E_p=24, 30.5, 35, and 45 MeV together with the results of microscopic DWBA calculations. (a) Results at E_p=45 MeV. The curves are calculated using Pot $A1$ (Table I) and Pot $1/1a$ (Table II) in zero-range and finite-range approximation and Pot $2/2a$ (Table II) in zero-range approximation. (b) Results at E_p=24, 30.5, 35, and 45 MeV. The curves are calculated using Pot $A2$ (Table I) and Pot $2/2a$ (Table II) in zero-range approximation.

TABLE V. Normalization factors ϵ_{ZR} and ϵ_{FR} as defined by Eqs. (50) and (51) for the reaction ^{27}Al(p,α)^{24}Mg(g.s.). Microscopic form factor.

E_p/(MeV)	Optical α potential (Table I)	Bound state potential (Table II)	ϵ_{ZR}	ϵ_{FR}
45	Pot $A1$	Pot $1/1a$	69	213
45	Pot $A1$	Pot $2/2a$	62	201
45	Pot $A2$	Pot $2/2a$	89	
35	Pot $A2$	Pot $2/2a$	94	
30.5	Pot $A2$	Pot $2/2a$	98	
24	Pot $A2$	Pot $2/2a$	74	

independent potential Pot $A1$ and the energy-dependent potential Pot $A2$ at E_p=45 MeV one finds different shapes in the theoretical curves. Besides, the normalization factors differ by a factor of 1.5. These differences indicate the crucial influence of the choice of the optical α potentials.

However, the theoretical curves calculated with the energy-dependent α-potential Pot $A2$ fit the data at the four energies with comparable quality [Fig. 6(b)]. As a further result, it is remarkable that the value of the normalization factors are nearly independent of the incident energy (Table V). That means that the cross section of the ground state transition of the ^{27}Al(p,α)^{24}Mg reaction can be reasonably well described in a large range of incident energies using a microscopic theory.

However, the theoretical cross sections are about two orders of magnitude too small when compared to the experimental data. This result has also been obtained in DWBA analyses of other (p,α) reactions[54] and a similar situation is found in (p,t) reactions[55] where the cross sections are typically too small by at least an order of magnitude.

This discrepancy may be due to the following reasons:

(1) Contributions from sequential transfer processes may be of comparable importance and even dominant to single-step processes. This has been shown already in (p,t) processes where the inclusion of sequential transfer enhances the cross section significantly.[56] On the other hand, the sequential transfer amplitudes are remarkably similar to simultaneous transfer amplitudes, and this means that the shape of the angular distributions and the relative cross sections are not altered by including sequential transfer processes.[55]

(2) The absolute cross section value is very sensitive to the choice of the optical α potential. By using shallow potentials the value of the normalization factor is improved. However, the shapes of the angular distributions of the cross sections, as well as the analyzing powers, cannot be reproduced.[54,57]

(3) For (p,t) reactions the choice of realistic nucleon-nucleon potentials and triton wave functions, as well as the inclusion of two-particle correlations in the bound-state wave function of the transferred nucleon pair, leads to agreement with experiment.[58] In (p,α) reactions the consideration of two-nucleon correlations may also result in an enhancement of the wave function of the transferred

nucleons at the nuclear surface. This has already been shown in (p,t) reactions by using an extended basis shell model.[59] The center-of-mass correction of the shell-model wave functions also tends to increase the wave functions at the nuclear surface.[60] The enhancement caused by those two effects can be studied in an empirical way by varying the geometrical parameters of the form factor. This point will be discussed in the next subsection using the semimicroscopic model.

B. Semimicroscopic analysis of the ground state transition

We have performed semimicroscopic DWBA calculations using cluster form factors calculated in a Woods-Saxon potential and multiplied with the SU(3) spectroscopic amplitudes based on the same shell-model wave functions as the microscopic ones. Some resulting angular distributions are shown in Fig. 7 together with the experimental data already given in Fig. 6. The corresponding normalization factors are summarized in Table VI together with the geometrical parameters of the Woods-Saxon potentials needed to calculate the cluster form factors. In our analysis only the radius parameter r_0 has been varied.

In Fig. 7(a) the data at $E_p=45$ MeV are analyzed in zero-range DWBA using the optical α potential Pot $A1$. In Fig. 7(b) the results calculated with the optical potential Pot $A2$ are shown. As shown in Fig. 7, the calculated curves show different slopes in the angular distributions which strongly depend on the radius parameter r_0 of the Woods-Saxon potential used. The normalization factors ϵ_{ZR} show a strong decrease with increasing radius parameter r_0 (Table VI).

We made three choices for the radius parameter r_0 of the cluster bound-state potential. The radius parameter $r_0=1.1$ fm was chosen, since in this case the hybrid and the cluster form factor agree in the region outside the nuclear surface. Comparing Figs. 6(a) and 7(a) one can see that the slope of the resulting angular distribution calculated with the cluster form factor is different to that cal-

TABLE VI. Normalization factors ϵ_{ZR} as defined by Eq. (51) for the reaction ^{27}Al(p,α)^{24}Mg(g.s.). Cluster form factor.

	Optical α potential	Cluster potential		
E_p/(MeV)	(Table I)	r_0/(fm)	a/(fm)	ϵ_{ZR}
45	Pot $A1$	1.1	0.55	30
45	Pot $A1$	1.32	0.55	6.2
45	Pot $A1$	1.95	0.55	0.10
45	Pot $A2$	1.32	0.55	6.7
35	Pot $A2$	1.32	0.55	7.2
30.5	Pot $A2$	1.32	0.55	7.8
24	Pot $A2$	1.32	0.55	6.6
45	Pot $A2$	1.95	0.55	0.11
35	Pot $A2$	1.95	0.55	0.09
30.5	Pot $A2$	1.95	0.55	0.10
24	Pot $A2$	1.95	0.55	0.05

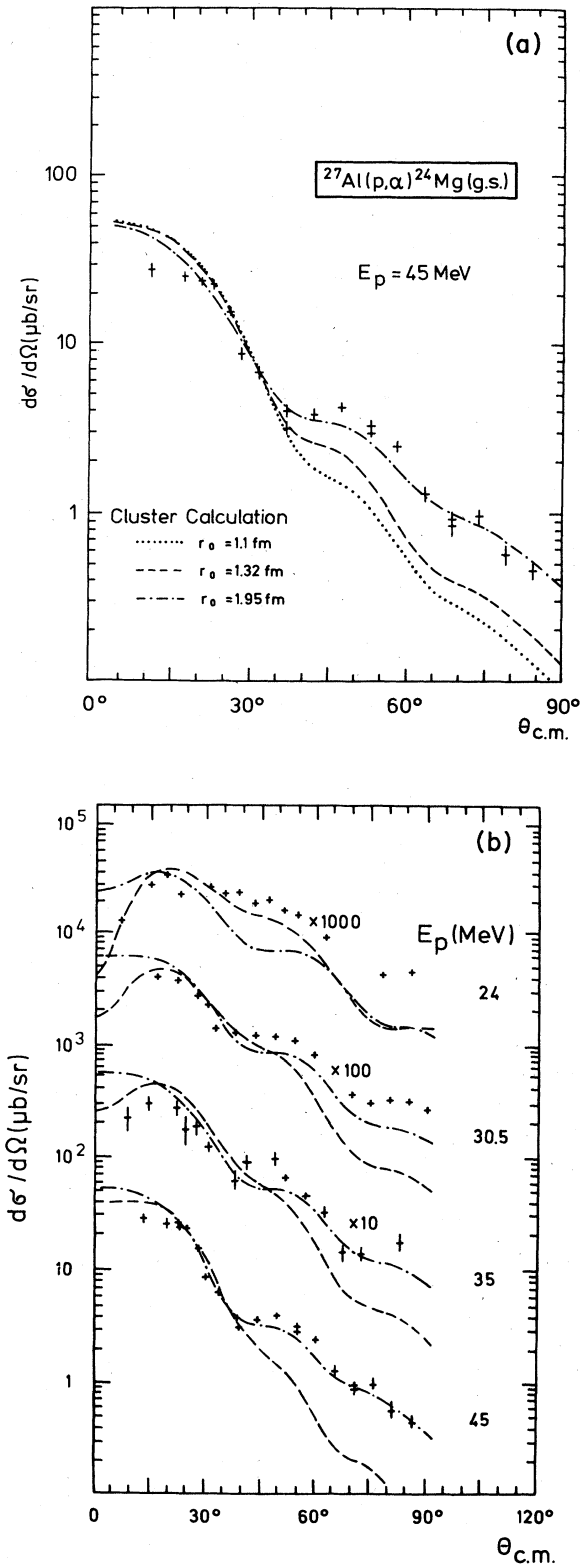

FIG. 7. Same as Fig. 6 but with the results of semimicroscopic DWBA calculations. (a) Same as Fig. 6(a), but the curves are calculated using cluster form factors with different bound-state radii (Table VI) in zero-range approximation. (b) Same as Fig. 6(b), but the curves are calculated with cluster form factors (Table VI) in zero-range approximation.

culated with the hybrid form factor. These differences, therefore, indicate the influence of the inner nuclear region to the (p,α) reaction. The resulting normalization factors, however, are of the same order of magnitude in both calculations.

The radius parameter $r_0=1.32$ fm was chosen, since this value is similar to that used in the microscopic calculations of the single-particle wave functions. The resulting angular distributions are very similar to those obtained in the microscopic calculations. The best fit to the experimental data at $E_p=30.5$, 35, and 45 MeV is found using a cluster form factor with $r_0=1.95$ fm. A similar large value has been required in earlier analyses of (p,α) reactions on light nuclei.[19]

Concluding these results, it can be stated that the shape of the angular distributions can be well fitted by semimicroscopic calculations. Using energy-dependent optical potentials the resulting normalization factors are nearly constant in a large range of incident energies. But the adjustment of the radius parameter gives a large variation of the theoretical cross sections. Only when the cluster form factor agrees with the hybrid form factor in the outer nuclear region, are the normalization factors in the microscopic and semimicroscopic analyses of the same order of magnitude.

The enhancement of the cluster form factor at the nuclear surface and the outer region caused by a larger radius parameter r_0 tends to decrease the normalization constant significantly. In the microscopic model such an enhancement may originate from two-body correlations and center-of-mass corrections in the bound-state wave function as already mentioned.

C. Spectroscopic results for transitions to excited states in ^{24}Mg

The analysis of the transitions to the excited states of ^{24}Mg is rendered more difficult due to the spin $\frac{5}{2}$ of the target nucleus ^{27}Al, since only transitions to spin 0 states have a unique angular-momentum transfer. To perform DWBA calculations for the transitions to the excited states in ^{24}Mg the components of the individual J transfer have to be added incoherently. Because of the enormous number of three-particle configurations involved, no microscopic calculations have been attempted.

In the zero-range semimicroscopic calculations a Woods-Saxon potential was used for the cluster bound state with the parameters $r_0=1.35$ fm and $a=0.55$ fm. The individual J components have been multiplied with the SU(3) spectroscopic amplitudes given in Table IV. The optical potentials Pot P and Pot $A2$ are used in these calculations.

The results are shown in Fig. 8 for the incident energies $E_p=30.5$ and 45 MeV. As one can see from Table VII, all transitions yield a nearly constant normalization factor with the exception of the transition to the first excited 2^+ state. For this transition the strength given by theory is underestimated by nearly a factor of 2.

The comparison between the experimental integrated cross sections and theoretical results is shown for $E_p=45$ MeV in Fig. 9. The open bars represent the experimental

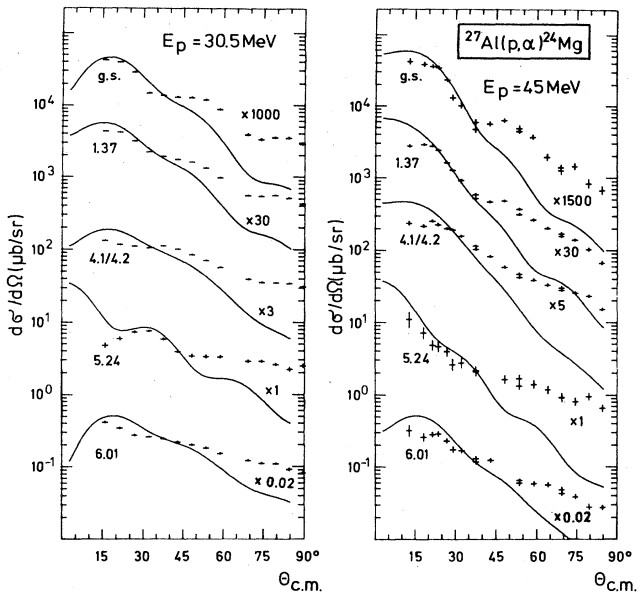

FIG. 8. Differential cross sections of the reaction ^{27}Al(p,α)^{24}Mg at $E_p=30.5$ and 45 MeV leading to the ground state and to excited states in ^{24}Mg. The solid lines are the result of semimicroscopic DWBA calculations using cluster form factors and SU(3) spectroscopic amplitudes (Table IV).

data integrated between 13° and 84°, and the crossed bars represent the corresponding DWBA values. As shown in previous investigations of the (p,α) reaction on light nuclei,[19] the relative intensities can also be described by the bare SU(3) spectroscopic factors. This is confirmed by the solid black bars which represent the sum over the squared spectroscopic amplitudes as given in the last column of Table IV. The similarity of the DWBA values with the sum of the squared SU(3) spectroscopic amplitudes shows the minor importance of the dynamics of the (p,α) process for the relative transition intensities. This result becomes still more evident if one compares the results of the ^{27}Al(^{3}He,^{6}Li)^{24}Mg reaction[61] to the (p,α) reaction. These results have been marked as shaded bars in Fig. 9. All results have been normalized to the ground state transition.

As shown by Buck *et al.*,[19] one expects the reaction ^{27}Al(p,α)^{24}Mg to be predominantly direct at proton energies higher than 20 MeV. This result together with the

TABLE VII. Normalization factors ϵ_{ZR} as defined by Eq. (51) and relative normalization constants $\epsilon_{ZR}(\text{rel})=\epsilon_{ZR}/\epsilon_{ZR}(\text{g.s.})$.

E_x/(MeV)	J^π	ϵ_{ZR}	ϵ_{ZR}(rel)	ϵ_{ZR}	ϵ_{ZR}(rel)
		$E_p=45$ MeV		$E_p=30.5$ MeV	
g.s.	0^+	5.00	1	4.53	1
1.37	2^+	8.34	1.67	7.94	1.75
4.12	4^+	5.78	1.16	5.12	1.13
4.24	2^+				
5.24	3^+	3.75	0.75	3.16	0.70
6.01	4^+	4.06	0.81	3.48	0.77

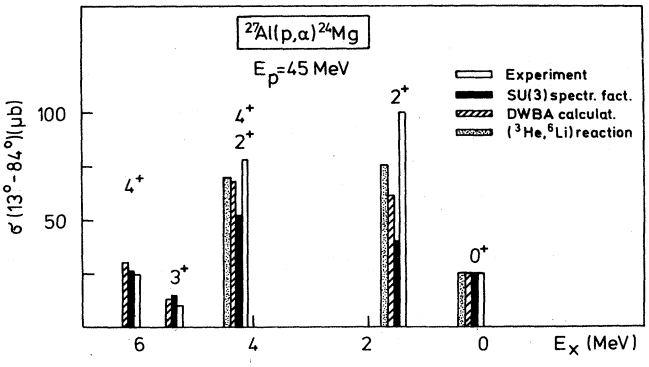

FIG. 9. Comparison of the experimental cross sections σ_{exp} of the reaction ^{27}Al(p,α)^{24}Mg at E_p=45 MeV, integrated from 11° to 84° (open bars), the corresponding theoretical values (crossed bars), the sum of the squared spectroscopic amplitudes (solid bars), and the experimental cross sections of the reaction ^{27}Al(^{3}He,^{6}Li)^{24}Mg integrated between 0° and 90° (shaded bars). The data are normalized to the ground state transition.

result given already also justifies the comparison of the experimental integrated cross sections with the spectroscopic factors at the rather low proton energy of 20 MeV as shown in Fig. 10. Again the open bars represent the experimental data and the solid bars the sum of the squared spectroscopic amplitudes given in Table IV. The theoretical values are normalized to the ground state. Up to an excitation energy of 6 MeV, the correspondence between theory and experiment is as good as at 45 MeV. In agreement with the theoretical prediction the 0^+ state at 6.43 MeV could not be observed in the experiments at 30.5 and 45 MeV. Therefore the observed intensity of this transition at 20 MeV provides an estimate of the importance of the compound process at lower energies. With exception of the 1^+ state at 7.75 MeV, one can observe a fair agreement between experiment and the theoretical prediction for the strengths of the positive parity states in ^{24}Mg also at excitation energies higher than 6 MeV.

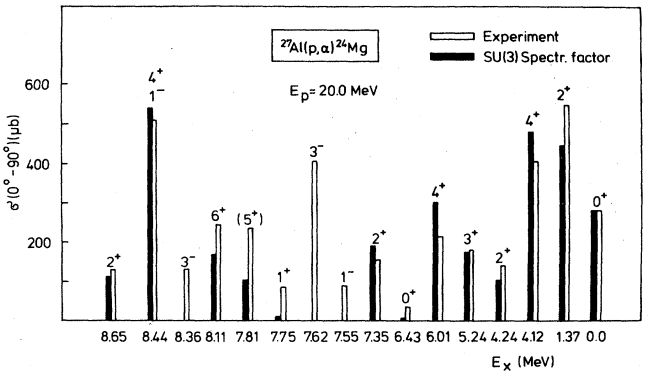

FIG. 10. Comparison of the experimental cross section σ_{exp} of the reaction ^{27}Al(p,α)^{24}Mg integrated between 0° and 90° (open bars) and the sum of the squared spectroscopic amplitudes (solid bars). The data are normalized to the ground state transition.

VI. CONCLUSION

The investigation of three-nucleon transfer reactions can be carried out by either using a microscopic or semimicroscopic analysis. In the microscopic model only parameters are used, which are taken from general systematics independent of the transfer reaction discussed. In the semimicroscopic model considered the SU(3) spectroscopic amplitudes, based on the same shell-model wave functions as the microscopic ones, are combined with cluster form factors. Since the cluster form factors have adjustable geometrical parameters in the bound-state potential, the shapes of the experimental angular distribution can usually be better reproduced. Furthermore, cluster form factors are easier to calculate than microscopic ones. One aspect of the present paper is to compare the microscopic and semimicroscopic analyses.

The microscopic as well as the semimicroscopic DWBA analysis of the reaction ^{27}Al(p,α)^{24}Mg reproduce the angular distributions in the range between 24 and 45 MeV when energy-dependent optical potentials are used. Likewise, the normalization factors are almost energy independent.

However, in the microscopic analysis the normalization factor is about two orders of magnitude too large. This may be attributed to the neglect of sequential transfer and of two-nucleon correlations and center-of-mass corrections in the bound-state wave function. It is well known from (p,t) reactions that the use of realistic bound-state wave functions enhances the form factor at the nuclear surface. We have simulated this enhancement by increasing the radius parameter in the semimicroscopic model and have found a significant reduction of the normalization factor.

The relative intensities of the transitions to the ground state and to excited states in ^{24}Mg can be well described in the semimicroscopic DWBA using SU(3) spectroscopic amplitudes. Beyond it, the strengths can be reproduced by the sum of the spectroscopic amplitudes alone even for a projectile energy of 20 MeV. This result indicates the minor importance of the reaction dynamics for the relative transition intensities.

ACKNOWLEDGMENTS

We are very grateful to Dr. W. Chung for providing us with the values of the spectroscopic amplitudes. Thanks are expressed to the tandem group of the MPI für Kernphysik, Heidelberg, and to the cyclotron group of the Institute for Nuclear Physics, KFA, Jülich, for the operation of the accelerators. We would like to thank the scanning team of the MPI für Kernphysik for the analysis of the nuclear track plates. One of us (H.O.) expresses his appreciation to the Alexander von Humboldt-Stiftung for a fellowship at the University of Tübingen. This work was supported by Bundesministerium für Forschung und Technologie.

*Permanent address: Institut für Kernphysik, Technische Universität, Wien, Austria.
[1]B. F. Bayman, Argonne National Laboratory Report ANL-6878, 1964, p. 335.
[2]J. A. Nolen, Jr., Ph.D. thesis, Princeton University, 1965.
[3]R. O. Ginaven, Ph.D. thesis, MIT, 1966.
[4]W. R. Falk, Phys. Rev. C **8**, 1757 (1973); W. R. Falk, A. Djaloeis, and D. Ingham, Nucl. Phys. **A252**, 452 (1975).
[5]B. F. Bayman and A. Kallio, Phys. Rev. **156**, 1121 (1967).
[6]P. A. Smith, Ph.D. thesis, Michigan State University, 1978.
[7]B. F. Bayman, A. Evinay, C. Ellegard, J. D. Garrett, and O. Hansen, Nucl. Phys. **A318**, 317 (1979).
[8]W. R. Falk, R. Abegg, and S. K. Datta, Nucl. Phys. **A334**, 445 (1980).
[9]H. Oberhummer, Nuovo Cimento **55A**, 253 (1980).
[10]P. D. Kunz, T. Kammuri, and H. Shimaoka, Nucl. Phys. **A376**, 401 (1983).
[11]H. Oberhummer, W. Pfeifer, F. Brunner, and H. H. Müller, Nucl. Phys. **A401**, 415 (1983).
[12]P. A. Smith and R. J. Peterson, Nucl. Phys. **A363**, 287 (1981).
[13]J. W. Smits and R. H. Siemssen, Nucl. Phys. **A261**, 385 (1976); J. W. Smits, thesis, University of Groningen, 1977.
[14]M. Ichimura, A. Arima, E. C. Halpert, and T. Terasawa, Nucl. Phys. **A204**, 225 (1973).
[15]J. B. McGrory, Phys. Lett. **47B**, 481 (1973).
[16]K. T. Hecht and D. Braunschweig, Nucl. Phys. **A244**, 365 (1975).
[17]D. Kurath and D. J. Millener, Nucl. Phys. **A238**, 269 (1975).
[18]K. van der Borg, R. J. de Meijer, and A. van der Woude, Nucl. Phys. **A273**, 172 (1976); C. R. Bingham, K. van der Borg, R. J. de Meijer, and A. van der Woude, Nucl. Phys. **A323**, 26 (1979).
[19]W. Buck, F. Hoyler, A. Stäbler, G. Staudt, and H. V. Klapdor, Nucl. Phys. **A398**, 189 (1983).
[20]C. C. Maples and J. Cerny, Phys. Lett. **38B**, 504 (1972).
[21]S. Abdel Kariem, H. J. Hauser, G. Staudt, M. Walz, and P. Turek, Verh. Dtsch. Phys. Ges. (VI) **17**, 1207 (1982).
[22]R. K. Bhowmik, J. A. Nolen, Jr., P. A. Smith, R. G. Markham, and M. A. M. Shahabuddin, Bull. Am. Phys. Soc. **20**, 1164 (1975).
[23]H. J. Hauser, F. Hoyler, H. Oberhummer, T. Rohwer, F. Brunner, H. Müller, P. Schober, and H. Cech, Verh. Dtsch. Phys. Ges. (VI) **17**, 1265 (1982).
[24]F. Hoyler, T. Rohwer, G. Staudt, H. V. Klapdor, and P. Turek, Verh. Dtsch. Phys. Ges. (VI) **15**, 1224 (1980); F. Hoyler, T. Rohwer, G. Staudt, H. V. Klapdor, P. Turek, and S. Martin, *ibid.* **16**, 649 (1981); T. Rohwer, W. Oelert, and P. Turek, *ibid.* **17**, 1207 (1982).
[25]C. J. Kost and B. Hird, Nucl. Phys. **A132**, 611 (1969).
[26]I. S. Towner and J. C. Hardy, Adv. Phys. **18**, 401 (1969).
[27]N. K. Glendenning, Phys. Rev. **137**, B102 (1965).
[28]H. Guyer, V. Meyer, H. H. Müller, W. Reichart, H. Oberhummer, P. Riehs, R. Wagner, and W. Pfeifer, Phys. Rev. C **18**, 1626 (1978).
[29]N. S. Chant and N. F. Mangelson, Nucl. Phys. **A140**, 81 (1970).
[30]Y. F. Smirnov, Nucl. Phys. **27**, 177 (1961); **39**, 346 (1962).
[31]J. R. Shepard, W. R. Zimmerman, and J. J. Kraushaar, Nucl. Phys. **A275**, 189 (1977).
[32]L. S. August, P. Shapiro, L. R. Cooper, and C. D. Bond, Phys. Rev. C **4**, 2291 (1973).
[33]H. Leeb, Technical University, Wien, Computer code GOMFIL (unpublished).
[34]H. S. Sandhu, Nucl. Phys. **A146**, 163 (1970).
[35]F. D. Becchetti and G. W. Greenlees, Phys. Rev. **182**, 1190 (1969).
[36]J. Lega and P. P. Macy, Nucl. Phys. **A218**, 429 (1974).
[37]G. R. Satchler, Nucl. Phys. **70**, 177 (1965).
[38]N. Baron, Phys. Rev. C **4**, 1159 (1971).
[39]H. H. Duhm, Nucl. Phys. **A118**, 563 (1968).
[40]F. Michel, J. Albinski, P. Belery, Th. Delbar, Gh. Gregoire, B. Tasiaux, and G. Reidemeister, Phys. Rev. C **28**, 1904 (1983).
[41]W. R. Smith, Comput. Phys. Commun. **1**, 55 (1970).
[42]K. Bear and P. E. Hodgson, J. Phys. G **4**, L287 (1978).
[43]F. Malaguti and P. E. Hodgson, Nucl. Phys. **A215**, 243 (1973).
[44]A. Insolia, M. Baldo, F. Catara, and A. Vitturi, Z. Phys. A **301**, 209 (1981).
[45]W. Falk, University of Manitoba, Computer code FORM, modified by H. Oberhummer (unpublished).
[46]H. Oberhummer, Technical University, Wien, Computer code FFR (unpublished).
[47]C. C. Bennett, Nucl. Phys. **A284**, 301 (1977).
[48]W. Chung, private communication.
[49]W. Chung and B. H. Wildenthal, private communication.
[50]M. Harvey, in *Advances in Nuclear Physics,* edited by E. Baranger and E. Vogt (Plenum, New York, 1968), Vol. 1, p. 67.
[51]P. D. Kunz, University of Colorado, computer code DWUCK V (unpublished).
[52]P. D. Kunz, University of Colorado, computer code DWUCK IV (unpublished).
[53]F. Brunner, H. Cech, H. H. Müller, G. Ratel, H. Jasicek, and H. Oberhummer, J. Phys. G **6**, 473 (1980).
[54]F. Brunner, H. H. Müller, C. Dorninger, and H. Oberhummer, Nucl. Phys. **A398**, 84 (1983).
[55]W. T. Pinkston, Comments Nucl. Part. Phys. **12**, 133 (1984).
[56]S. Kunori, Y. Aoki, H. Ida, K. Nagano, and Y. Toba, Phys. Rev. Lett. **46**, 810 (1981).
[57]J. J. Hamill and P. D. Kunz, Phys. Lett. **129B**, 5 (1983).
[58]D. H. Feng, M. A. Nagarajan, M. R. Strayer, M. Vallieres, and W. T. Pinkston, Phys. Rev. Lett. **44**, 1037 (1980).
[59]W. T. Pinkston, M. Vallieres, and D. H. Feng, Phys. Rev. C **18**, 1011 (1978).
[60]W. T. Pinkston and P. J. Iano, Nucl. Phys. **A330**, 91 (1979).
[61]I. K. Oh, C. S. Zaidius, C. D. Zafiratos, and S. I. Hayakawa, Nucl. Phys. **A178**, 497 (1972).
[62]C. M. Perey and F. G. Perey, At. Data Nucl. Data Tables **17**, 1 (1976).